Proceedings of International Conference on Heat Exchanger Fouling and Cleaning - 2011 (Peer-reviewed)
June 05 - 10, 2011, Crete Island, Greece
Editors: M.R. Malayeri, H. Müller-Steinhagen and A.P. Watkinson

EXHAUST GAS RECIRCULATION COOLER FOULING IN DIESEL APPLICATIONS: FUNDAMENTAL STUDIES, DEPOSIT PROPERTIES AND MICROSTRUCTURE

J.M.E. Storey,[1] C.S, Sluder[1], M.J. Lance[1], D. Styles[2], and S. Simko[2]

[1] Oak Ridge National Laboratory, P.O. Box 2008, M.S. 6472, Oak Ridge, TN 37831-6472. storeyjm@ornl.gov
[2]Ford Motor Company, RIC Building, P.O. Box 2053, Dearborn, MI 48121-2053

ABSTRACT

This paper reports on the results of experimental efforts aimed at improving the understanding of the mechanisms and conditions at play in the fouling of EGR coolers. An experimental apparatus was constructed to utilize simplified surrogate heat exchanger tubes in lieu of full-size heat exchangers. The use of these surrogate tubes allowed removal of the tubes after exposure to engine exhaust for study of the deposit layer and its properties. The exhaust used for fouling the surrogate tubes was produced using a modern medium-duty diesel engine fueled with both ultra-low sulfur diesel and biodiesel blends. At long exposure times, no significant difference in the fouling rate was observed between fuel types and HC levels. Surface coatings for the tubes were also evaluated to determine their impact on deposit growth. No surface treatment or coating produced a reduction in the fouling rate or any evidence of deposit removal. In addition, microstructural analysis of the fouling layers was performed using optical and electron microscopy in order to better understand the deposition mechanism. The experimental results are consistent with thermophoretic deposition for deposit formation, and van der Waals attraction between the deposit surface and exhaust-borne particulate.

INTRODUCTION

Exhaust gas recirculation (EGR) in diesel engines is a commonly used strategy for pollutant reduction. The engine operating envelope where EGR is demanded is growing, as is the overall EGR fraction, and hence also the need for effective cooling of these gases over a wide range of flows and temperatures. Mitigating the fouling of these heat exchangers is a critical need for reducing the cost of diesel engines as well as enabling continued improvement of fuel efficiency and emissions performance. In most cases, the EGR flow is cooled before introduction into the intake. The exhaust particulate matter (PM) is driven to the cooler walls by thermophoresis resulting in the deposition of an insulating layer on the walls, and the loss of thermal efficiency of the cooler. Additionally, exhaust hydrocarbons (HC) migrate to the wall, and in some cases, can build up enough to completely plug individual heat exchanger tubes with sludge-like mixture of PM and HC. The fouling of these heat exchangers by diesel PM and HC has thus emerged as a formidable problem for the industry, and leads to loss of engine efficiency and warranty problems.

Earlier studies identified these effects in automotive EGR coolers. Lepperhoff and Houben (1993) described the fouling effect on heat exchangers and early EGR coolers. Others have developed methods for assessing fouling and metrics for performance degradation in EGR coolers (Bravo *et al.,* 2005, Ismail *et al.*, 2005.) Hoard *et al.* (2008) and Abd-Elhady *et al.* (2011) recently reviewed the literature on automotive EGR cooler fouling and detailed areas of research that were needed.

Our laboratory has been engaged in fundamental studies of the EGR fouling process for the past several years (Sluder et al., 2008, 2009). An apparatus, described by Styles et al. (2010) with removable cooler tubes was designed and used to expose tubes of simple geometry to diesel exhaust under a variety of exhaust conditions with the goal of understanding the importance of parameters such as temperature, flow rate, HC level, and surface modification on the degradation in thermal efficiency of the cooler and the mass of the deposit. Microstructural analysis was also performed on a subset of the tubes to characterize the PM deposit morphology and density.

Definition of Terms and Approach

The effectiveness (ε) of a heat exchanger is defined as the actual heat transfer divided by the maximum possible heat transfer. This can be further defined in terms of temperatures according to Equation (1).

$$\varepsilon = (T_{Gas\ In} - T_{Gas\ Out}) \,/\, (T_{Gas\ In} - T_{Coolant\ In}) \qquad (1)$$

The effectiveness, then, is the ratio of the actual change in temperature of the EGR gas stream divided by the maximum change in temperature that the EGR gas stream could have experienced by being cooled to the temperature of the coolant. Since actual heat transfer rate for a given heat exchanger depends upon the flow rates and properties of the gases and coolants, effectiveness also varies with these characteristics independent of fouling. Nevertheless, it is a useful measure of performance as it is easily calculated from measurable quantities.

Studies of in-use EGR coolers can facilitate long-term evaluations of the fouling process, but because of their size and physical layout, full-size coolers are inconvenient for studies of the fundamentals of the fouling process. Furthermore, as the coolers foul, the engine operating parameters are affected so that the fouling process and the cooler feedgas conditions are linked. This is, of course, the situation in practice; however, it is useful to study the fouling process with constant feedgas conditions to clarify relationships among key variables. Thus, a system was devised to utilize surrogate tubes to represent the EGR cooler for this study.

Most discussions concerning field-aged EGR coolers focus on the role of HCs behaving as an adhesive and in forming the refractory glazes and lacquers that cause many problems for manufacturers. In the surrogate tube studies our laboratory has performed, HCs appear to have an increased role in initial performance degradation but then, as the deposit layer thickens, little additional influence in the degradation of cooler effectiveness. Of course, these experiments only measure the short term effects of the HC; no attempts were made to reproduce the accumulation of sludge-like soot-HC mixtures in field-aged coolers.

This discussion will focus on the insulating nature of the deposits and some fundamental, physical explanations for the highly insulating nature of the deposits that are somewhat unique to the application of heat exchangers to diesel exhaust.

van der Waals attraction to surfaces

The adherence of PM to the EGR cooler tube walls is widely believed to be a result of van der Waals forces. van der Waals forces arise through the interaction of particles with electromagnetic fields; this results in temporary and time-dependent charges on the particles. When particles and the tube walls have opposite charges that are moving in phase with one another, a net attractive force arises (Parsegian, 2006.) The charges need not be uniform over the surface of the particle for this to occur; polarization can occur, for example, on one side of the particle as a result of the chemical structure of the particle. Exact calculation of the van der Waals energies of interaction is possible for simple geometries and known distances between particles. For the complex geometry of aggregates, making simplifying assumptions is necessary. Making the assumption that the surface areas that take part in van der Waals interactions are derived from spherical particles of 30 nm diameter allows estimation of the directional dependencies of the attractive forces. Figure 7 shows the attractive energy normalized to random thermal energy for two 30 nm diameter particles. The Hamaker coefficient was taken to be 6 x 10^{-20} joules. When the van der Waals attractive energy is equal in magnitude to random thermal energy no net attractive force is produced. This condition is denoted by the dashed horizontal line in Fig. 1. The estimates show the strong effect of both separation distance L, shown as a parameterization of the particle radius, and temperature.

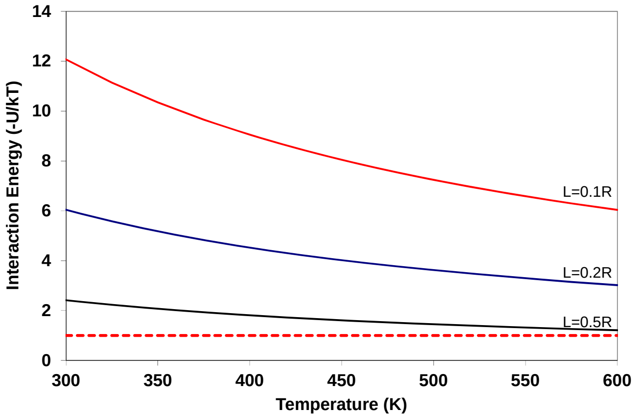

Fig. 1 van der Waals interaction energy normalized to random thermal energy for two spherical particles of 30 nm diameter.

It is clear from these estimates that the van der Waals interactions are strong as the deposit layer forms near the cooled tube wall and become weaker as the deposit increases in temperature. For example, the margin between the energy of interaction and random thermal energy for a separation distance equal to half the particle radius at 500K is only 32% of the same margin at 300K. This decrease in the net attractive force may cause a decreased deposition of PM as the deposit becomes hotter.

Idealized aggregate theory and deposit formation

Lall et al. (2006) developed idealized aggregate theory (IA) in order to model chain aggregates like those in engine exhaust. Barone et al. (2006) summarize IA in the following way: The concept of idealized aggregates applied to chains of particles is analogous to the use of the sphere to describe compact particles. The basic assumptions for idealized aggregates are as follows:

1. Aggregates are composed of primary particles all of which have the same diameter. This assumption is valid for modern DI engines because the primary particle size is influenced by the injector hole and the pressure of the fuel injection system.
2. The primary particles that compose the aggregates are much smaller than the mean free path of the surrounding gas. This corresponds to Knudsen numbers $Kn = 2k/dpp >> 1$ where k is mean free path of the gas and dpp is primary particle diameter. In many cases, the limit can be taken as $Kn \geq 10$. In our experience with diesel aggregates, primary particle sizes are typically 15-25 nm.
3. Aggregates are ‘‘transparent’’, that is, (nearly) all primary particle surfaces are directly exposed to collisions with molecules from the surrounding gas. This is an acceptable approximation for aggregates with fractal dimensions (Df) less than about two.

Madler et al (2006) determined porosities of a film (layer) of aggregate particles made up of 20 primary particles and showed that, for a wide range of primary particle sizes, 5 nm to 30 nm, the film porosity only varied from 0.98 to 0.99. Their study also showed that in the extreme limit of 2 primary particles per aggregate, the porosities were > 0.95. The microstructural results show that the aggregates that settle in our surrogate tubes have primary particle sizes on the order of 10-30 nm and many primary particles in a given aggregate.

The insulating nature, therefore of a layer of soot aggregates is well-founded in theory, and agrees with measurement. Measurements of surrogate tubes exposed to exhaust in our laboratory for 12 hours had an average thermal conductivity of 0.04 W/mK (Lance et al., 2009.) For reference, air is 0.025 W/mK, steel is 13 W/mK and the soot layer's thermal conductivity falls in the range of expanded polystyrene foams. This also agrees well with findings for carbon aerogels; Weiner at al. (2009) found that carbon aerogels with much larger micron-size primary particles had thermal conductivities of ~0.1 W/mK. Their research also finds that the largest contribution to thermal conductivity in very porous materials derives from the conductivity of the solid framework, as opposed to radiative heat transfer or diffusive heat transfer through the gas. By extension, the characteristic length scale for conductive heat transfer is not the deposit or film thickness, but rather the length of the tortuous path of the solid framework. Similarly, the characteristic surface area for heat transfer of a layer of aggregate particles depends on the primary particle diameter and the number of primary particle connections. In the case of EGR cooler soot layers, the solid framework has connections on the order of tens of nanometers as opposed to microns, so the characteristic heat transfer surface area is very low per individual framework.

With the introduction of HCs or water into the layer, the contact area can increase dramatically because of infiltration into the pores. This will increase the heat transfer area as well as shorten the characteristic length scale.

EXPERIMENTAL METHODS

A modern medium-duty diesel engine was used to generate exhaust for the surrogate tube exposure. The engine was operated at a condition consistent with a highway cruise condition, and the exhaust for the tube exposure was removed directly from the EGR loop prior to the EGR cooler entrance. Additional details of the engine can be found in Sluder et al. (2008).

Fuels and exhaust conditions

Experiments were carried out using ultra-low sulfur certification diesel (ULSD, Chevron-Phillips Specialty Chemical Company) and a 20% volume blend of soybean-derived biodiesel in ULSD (B20). The soy biodiesel used for these blends was obtained from SoyGold, a BQ9000-certified supplier.

The exhaust species of principal interest for this study were the PM level and the HC concentration. PM level was measured using a smoke meter (AVL model 415S); HC concentration was determined using a heated flame ionization detector (California Analytical model 300M). For the low HC experiments, the HC concentration was approximately 50 ppm and the smoke number 1.5 and 1.4 for the ULSD and B20 experiments, respectively. For the high HC experiments, all conditions were identical to the low HC experiments and an additional 50 ppm (reported as C1) of HC was added through nebulizing fuel into the gases immediately upstream of the surrogate tubes. For the ULSD experiments, the nebulized fuel was ULSD, for B20 experiments, it was B20.

Surrogate tubes

The surrogate tubes used for this study were made from 304 stainless steel. Both round (6.35 mm O.D., 0.89 mm wall) and square (6.35 mm side, 0.51 mm wall) cross-section tubes were used. The cooled length of the tube sections were 317 mm, and the tubes were designed for removal from the apparatus with minimal disturbance to the deposit. All microscopic imaging of the exhaust deposits was acquired on square cross-section tubes. Characterization of the tube surface and the coating morphologies were performed on round tubes. Given that the surrogate tubes are assemblies, other tube geometries are also possible, depending upon the goals of the study.

Four surrogate tubes were simultaneously exposed to exhaust conditions for each experiment in this study. Each tube had its own water jacket. The exhaust gas flow rate through each tube was individually controlled to a nominal 31 standard liters-per-minute (SLPM) rate, corresponding to 0.05 kg/min through each tube. The flow velocity was 20 m/s at the start of the experiment and increases to 24 m/s at the end of 8 hours due to the cross sectional area (and gas density) effects on the flow as the deposit thickness increases. The flow regime is turbulent under this condition. The engine conditions outlined previously produced tube inlet temperatures of ~375°C. Unless otherwise indicated, the coolant temperature was 90ºC. Additional details of the tube exposure rig are given in Styles et al. (2010).

Surrogate tube analysis

The tube thermal effectiveness was measured during the exposure to exhaust gases by monitoring the tube inlet temperature, tube outlet temperature, and coolant inlet temperature using type-K thermocouples. Gravimetric analyses of the deposits were carried out after the exposure was completed; total deposit mass gained was determined by first equilibrating the tubes at a constant temperature and relative humidity for >12 hrs prior to being weighed. This step was required to reduce errors associated with small changes in the amount of water present on the tube surfaces. Fractionation of the deposit mass into bins of volatility was accomplished by volatilizing the deposits in a tube furnace under an inert atmosphere of argon. Two high limit temperatures were used: 350 and 550°C. The 350°C limit compares favorably with the endpoint of the ULSD fuel distillation curve, while the 550°C limit removes other low-volatility HCs such as lubricating oil and polynuclear aromatic compounds. In general, very little mass was lost during the 550°C volatilization, and these results are presented elsewhere. (Sluder et al. 2008, 2009)

RESULTS

Surrogate tube fouling performance

In general, the fouling behavior and loss of effectiveness for the surrogate tubes was very uniform for a wide variety of flow rates and conditions. Figure 2 overlays fouling resistance curves from five separate experiments at a constant flow rate, but different exposure times. These represent the average of four tubes per experiment and demonstrate the repeatability of the experimental apparatus over shorter and longer exposure times. In addition, mass and density of the deposits were measured along the length of the model cooler tubes under 17 different deposition conditions. Results showed that there was no statistically significant change in deposition along the length of the cooler tubes.

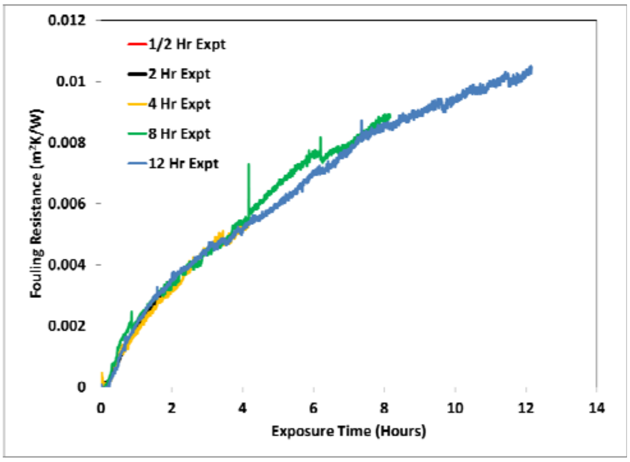

Fig. 2 Fouling resistance vs. time for five exposure times.

Effectiveness loss as a performance metric. Effectiveness loss was selected throughout the studies [Sluder et al, 2008, 2009; Styles et al. 2010] as a metric to quantify the loss of thermal performance of the tubes. Effectiveness loss was defined as the difference between the effectiveness at the end of the equilibration period minus the effectiveness at the end of the experiment. Using the effectiveness loss as a figure-of-merit removes from the analysis differences in effectiveness for each tube that may result from minor flow or manufacturing differences. This metric was calculated for each tube, then an average taken and confidence intervals established. As an example of this type of relationship, Fig. 3 below summarizes several tube exposure experiments where time, HC level, and fuel type were varied. Like Fig. 2, the effectiveness loss appears to be reaching a plateau. Although fuel and HC effects will be discussed later, it is important to point out in this figure that these effects diminish as exposure times increase and effectiveness loss reaches a plateau.

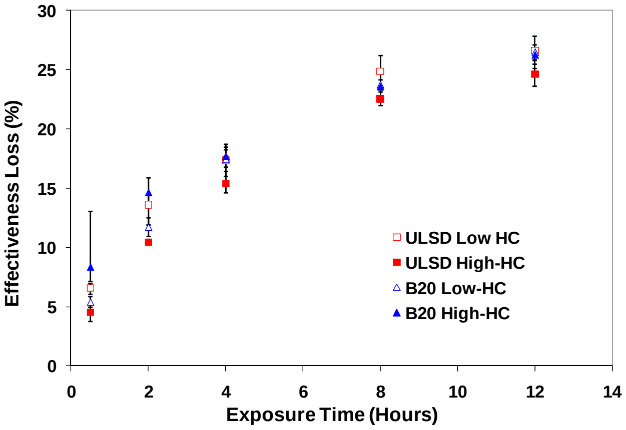

Fig. 3 Average effectiveness loss for each exposure time with two fuels, ULSD and B20, and two HC levels.

The error bars in Figure 3 represent the minimum and maximum values for the four tube samples in each experiment and thus shows that initial deposition (after 0.5 hours) leads to the most variation in effectiveness loss. This variation is quickly dampened and by 12 hours there is little difference in the values.

HC Effects. Exhaust HC are found in most EGR cooler deposits and, under some conditions, can accumulate to the point of clogging the passageways completely (Hoard *et al*, DEER 2007) with a mixture of soot and HC. To explore this phenomenon, experiments were done with the surrogate tubes under both low (~50 ppm nascent) HC conditions (Sluder 2008 SAE) and high HC conditions (Sluder, 2009 SAE), in which an additional 50 ppm C_1 equivalent of fuel was nebulized into the exhaust just prior to tube exposure. In general, only hydrocarbons less volatile than hexadecane (C_{16}) participate significantly in deposition. These types of compounds are usually found in the upper half of typical diesel fuel distillation. In Figure 4, the volatile fraction, defined as the fraction of the deposit mass that desorbs at 350°C, is plotted for the two levels of HC and the two fuels, ULSD and B20 as a function of exposure time. As exposure lengthens, the deposit mass increases, and the volatile fraction decreases, but appears to level out. Even at twelve hours, the absolute mass of HC in the deposit was still increasing so there appears to be some transfer to the cooler deposit layers near the walls.

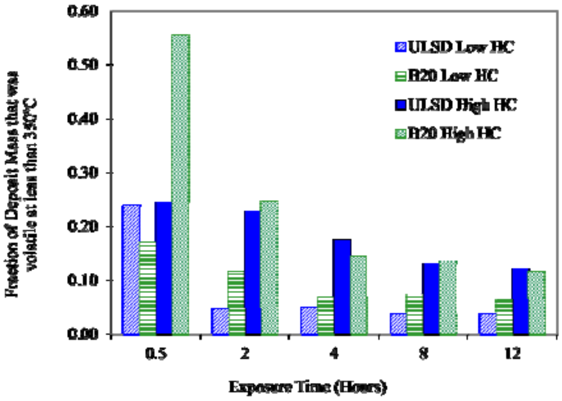

Fig. 4 Fraction of deposit mass that volatilized at 350°C as a function of exposure time.

Figure 5 shows the change in deposit density with exposure time for the high HC case. Density was measured on 1-inch segments of square tube by measuring the difference in mass before and after cleaning the deposit off and the deposit cross-sectional thickness which was used to calculate the deposit volume. The ULSD deposit maintains a constant density of 0.04 g/cm^3 over the entire range of exposure times whereas the B20 deposit starts off with a much higher density at one-half hour, due likely to the lower volatility of the biodiesel components, and then quickly reduces to the ULSD level at 4 hours and beyond. The density of the deposit is only slightly higher than air (0.025 g/cm^3) and so would correspondingly have a thermal conductivity similar to stagnant air.

Surface treatment effects on tube fouling

In order to investigate surface effects on the fouling of the surrogate tubes, tubes with five different surface treatments were prepared, including a base case 316 SS tube. The tubes in earlier studies were 304 SS.

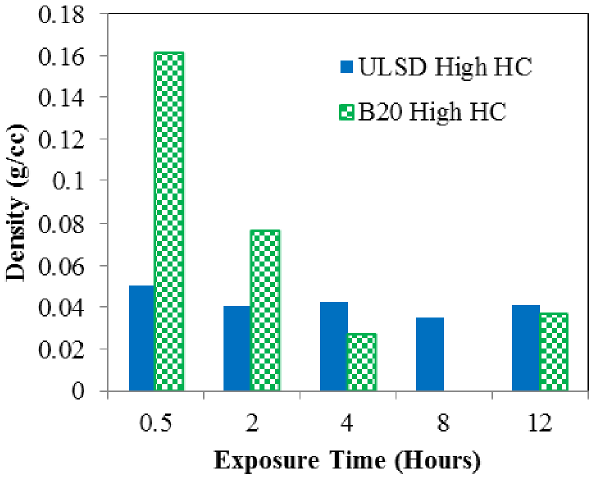

Fig. 5. The density of the high-HC deposit as a function of exposure time. The 8-hour B20 sample was damaged during milling and could not be measured.

The surface treatments included: electropolishing of the stainless steel; a nickel-Teflon® coating deposited via a spin-dip process; a preceramic polymer material that deposits silica-silicone coating; and an alumina-boron nitride coating deposited via a mechano-chemical deposition process. These coatings typically made the surface smoother but were thin enough to have a negligible effect on heat transfer.

The as-machined surfaces of the tubes were visually smooth, but exhibited extensive roughness on a microscale. Electro-polishing of the tube was tested to determine if reducing this micro-roughness would reduce the tendency for deposits to form. A significant reduction in surface roughness was achieved by this process as shown in the electron micrographs in Fig. 6 (images A and B). Coating the tubes also reduces the surface roughness somewhat as illustrated by the alumina-boron nitride coating shown in Fig. 6C. It is expected that these coatings would alter the surface chemistry so as to reduce the adherence of the deposit. The silica-silicone coating was chosen due to the fact that it is used by the petrochemical industry to prevent coking and so was suspected be beneficial here. Coating thicknesses were determined to be 0.9 µm thick (alumina-boron nitride coating), 1.6 µm thick (Ni-Teflon® coating), and 10 µm (preceramic coating) by examining the tubes prepared as metallurgical cross sections.

The tubes were exposed for four hours at the same conditions used in the previously described experiments (Sluder et al 2008, 2009). The fuel was certification ULSD, and the HC level was ~40 ppm nascent. Table 1 shows the results of the experiments which showed few effects, if any, for the coatings. Both mass deposition and effectiveness loss were similar for all of the tubes. The silica-silicone treated tubes are believed to have suffered thermal damage to the coating and thus showed less apparent weight gain, although the effectiveness loss was very close to that of stainless steel.

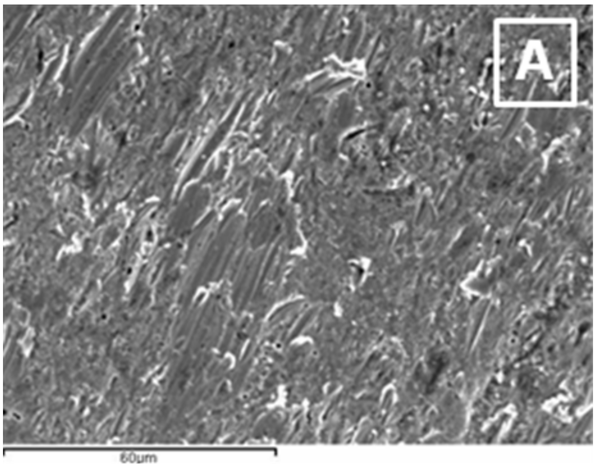

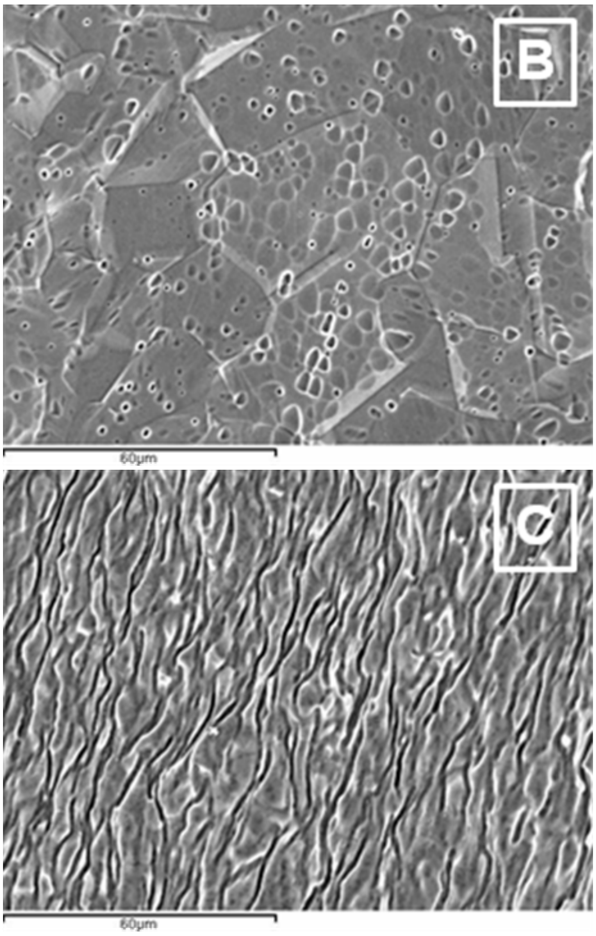

Fig. 6. Secondary electron images of the tubes prior to testing. Image A is the "as received" surface, image B is the tube after electropolishing, image C is the tube with the alumina-boron nitride coating. The image widths are all 130 µm.

Table 1. Mass gain and effectiveness loss for coated tubes

Tube type	Mass gain, mg/cm^2	Effectiveness loss, %
Plain 316 SS	0.598	16.7
Polished SS	0.598	17.9
Al_2O_3-BN	0.601	19.5
Ni-Teflon®	0.600	19.4
SiO_2-Si-O	0.303	16.9

Effect of deposit mass on performance In Fig. 3, both low- and high-HC conditions exhibited results that suggest little difference in the effectiveness loss resulting from differences in the fuel. In general, conditions that resulted in higher levels of volatiles in the deposit did not exhibit significantly higher or lower levels of effectiveness loss. Dividing the effectiveness loss by the total mass gain provides an indicator of the sensitivity of the effectiveness to deposit formation. This quantity is similar to a thermal resistance characteristic for the deposit layer. Figure 7 shows this data for both the low- and high-HC experiments, as well as for the coated tube experiments reported in Table 1. The data show that the deposits formed at high-HC conditions initially result in higher effectiveness losses than those formed at low-HC conditions. This effect is short-lived, and by 4 hours the high- and low-HC conditions provide deposits that have essentially the same loss of effectiveness on a deposit mass basis.

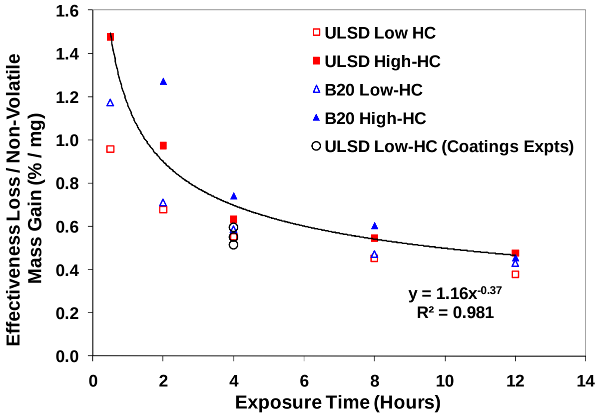

Fig. 7. Effectiveness normalized to mass gain for multiple tube exposure experiments

Microstructural results

As part of our investigation, it became clear that the structure and heat transfer properties of the deposit layer was critical to our understanding of the fouling process.

Figure 8A shows a cross-section of the 2-hour low-HC ULSD deposit formed on a square cross-section tube. The average thickness for this condition was 154 ± 28 µm. The cross-section was revealed by milling the tube to a thickness that allowed it to be carefully broken open, producing an unperturbed deposit fracture surface. In this image, the gas flow was normal to the fracture surface plane. At this magnification, the deposit appears to be dense but in reality the density of this deposit was measured to be only 0.045 g/cm3 which, using a theoretical density of the primary PM particles of 1.77 g/cm3 (Park et al. 2004), would give a porosity of 97.5%. The resulting thermal conductivity will be only slightly higher than air (Lance et al. 2009).

The low-HC deposits had at least two distinct microstructural regions: a thick denser bottom layer and a thin dendritic top layer. Figure 8B shows a high magnification image of this dendritic layer at the deposit-air interface that corresponds to the square from Figure 8A. The dendrites are 10s of microns tall and therefore must be composed of many PM aggregates from the exhaust. Looking at the top of this deposit, the dendrites appeared to cover less than half of the deposit surface. Also, when observing a fracture plane parallel to the exhaust flow, the dendrites appeared to be leaning in the flow direction. The dendrites can be clearly seen at 30 minutes and 2 hours but appear less clear at 4 hours and disappear entirely at 12 hours. In addition, the dendrites were not observed on the high-HC deposit.

One possible explanation of this phenomenon is that PM initially deposits randomly on the surface. Subsequent PM aggregates are caught by the initial aggregates through mechanical interlocking forming dendrites that grow perpendicular to the surface. Once a critical mass and height is reached, the gas flow will topple the dendrite, fracturing it at its base. The toppled dendrites will lay flat on one another forming the denser bottom layer. New PM aggregates from the gas will then randomly deposit in the new 'open' area formed following dendrite toppling. This process will repeat itself as the deposit thickens. Owing to the low thermal conductivity of the deposit, the deposit-gas interface temperature will increase as the deposit grows which will cause the dendrites to have a lower shear strength causing them to fracture at a shorter height. In addition, the exhaust velocity will increase as the tube cross-section narrows due to deposit growth which increases the shear force on the dendrites. Therefore, this deposit growth mechanism, PM trapping due to mechanical interlocking, is mostly deactivated after 12 hours causing the deposition, and hence the thermal effectiveness loss, to reach a plateau.

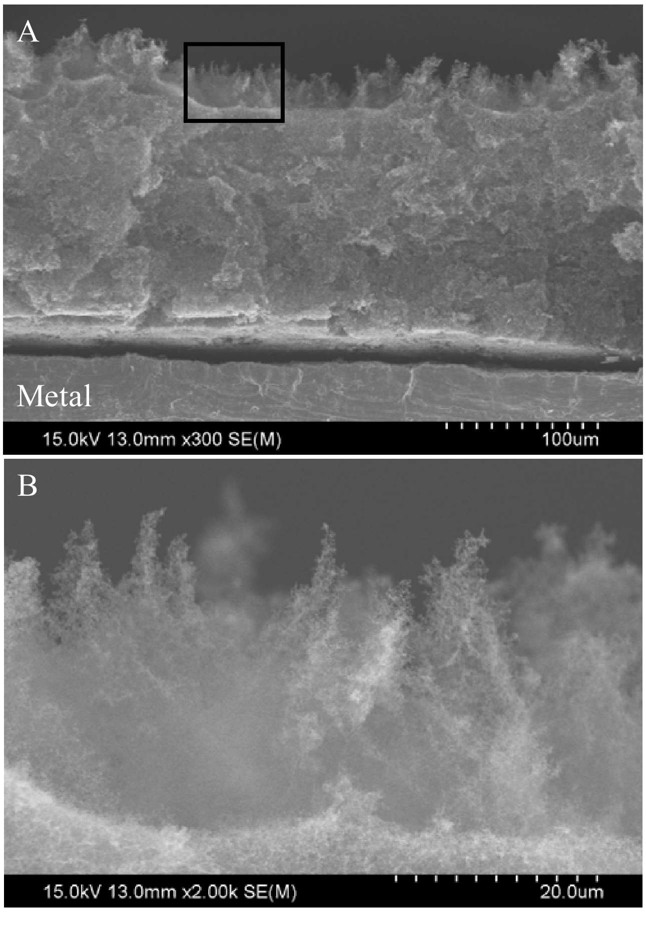

Fig. 8. Deposit formed after 2 hours of operation with 50 ppm ULSD HC. Both a low magnification image (A) and a high magnification image (B) demonstrating the dendritic top layer are shown. The region enclosed in the box in (A) corresponds to the region shown in (B).

Figure 8A shows that as the tubes are opened, the deposit will usually peel off the metal substrate producing a fracture plane near the metal-deposit interface. At higher magnifications, the metal adjacent to this fracture plane is typically covered with a dusting of PM. This suggests that at least for this uncoated tube surface and these deposition conditions, the PM to PM bond is weaker than the PM to metal bond. This tendency of the deposit to delaminate along a fracture plane that runs through the deposit as opposed to the deposit-metal interface was also observed on many industry-provided late-stage deposits discussed in Lance et al. (2010).

Figure 9 shows the deposit microstructure at the metal-deposit interface from an undelaminated region of a high-HC B20 deposit with the coolant temperature at 40°C formed after 2 hours on an uncoated tube. The dashed line shows the location of the metal-deposit interface as determined by back-scattered electron microscopy. The deposit microstructure becomes coarser near the metal. In addition, there appears to be a fully-dense layer a few microns thick coating the deposit. These microstructural features must be due to the presence of hydrocarbon species at and near the metal surface since the cold metal wall will promote the condensation and retention of heavy hydrocarbon species present in the exhaust gas. Structures similar to this were observed on all of the deposits discussed in this paper however, the location, morphology and prevalence of the coarser HC-rich regions varied significantly depending on the operating conditions. The presence of a fully-dense HC coating on the metal as seen in Fig. 9 was often hard to observe due to the roughness of the as-received surface. Nevertheless, it is expected that there will always be some HC present on metal surfaces cooled to 90°C or below due to the high boiling point of heavy HC species present in the exhaust gas. The amount of HC near the metal was difficult to quantify from the images however there did appear to be more HC with lower coolant temperatures (especially 40°C) and in one case where the HC was increased to 250 ppm, more than half the deposit thickness was comprised of a coarser microstructure where the PM appeared to be collapsed into dense columnar structures.

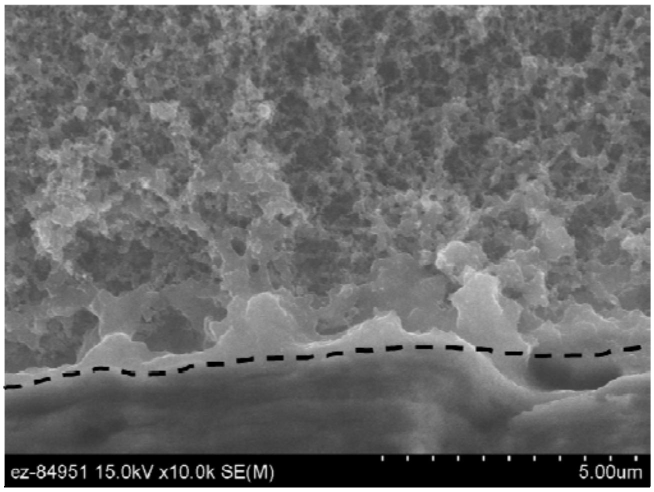

Fig. 9. The microstructure of a deposit produced with 100 ppm B20 HC and a coolant temperature of 40°C. The dashed line corresponds to the metal-deposit interface.

Two possible HC deposition mechanisms may be occurring. First the HC may condense on the metal only prior to PM buildup, perhaps aiding in the sticking of PM to the substrate. As the PM deposits, the HC may wick into the soot adjacent to it. The cooler the metal, the farther the HC can wick into the deposit before it volatilizes in the hotter upper deposit. Conversely, the HC may diffuse through the deposit as it grows and will condense on both the PM and the metal that is below its dew point isotherm.

CONCLUSIONS

1. Use of a surrogate tube sampler in place of an actual EGR cooler allowed for independent and repeatable control of key factors impacting EGR cooler fouling. The tubes are also easily removed for post test analysis.
2. The heat transfer effectiveness loss of the surrogate tubes appeared to be reaching plateau.
3. Higher HC levels initially resulted in greater deposit mass accumulation and increased deposit density but at later time intervals the deposit mass gain and density was similar to lower HC experiments.
4. Neither various "anti-stick" tube coatings/surface treatments or B20 fuel versus ULSD fuel appeared to have any significant impact on effectiveness loss or deposit mass gain for these experiments.
5. The soot deposits in EGR coolers are actually PM aggregates which form a highly porous deposit layer, with thermal conductivities in the range of 0.04 W/mK (similar to expanded polystyrene foam insulation).
6. The resulting increase in deposit layer temperature as this porous PM layer builds weakens the van der Waals which are understood to be the primary soot adherence force.
7. The weakened attraction along with decreased shear strength of the PM aggregates in the higher temperature outer extremities of the deposit layer may explain the asymptotic behavior of the loss of heat transfer effectiveness.

NOMENCLATURE

B20	20% biodiesel in ULSD
C1	Hydrocarbon with one carbon atom
Df	fractal dimension
DI	direct injection
dpp	diameter of primary particle, nm
ε	effectiveness
EGR	exhaust gas recirculation
HC	hydrocarbons
ID	inner diameter, mm
k	mean free path, nm
Kn	Knudsen number, dimensionless
L	Separation distance
OD	outer diameter, mm
PM	particulate matter
T	temperature
ULSD	ultra-low sulfur diesel

REFERENCES

M. S. Abd-Elhady, M.R. Malayeri, and H. Müller-Steinhagen, 2011, Fouling Problems in Exhaust gas Recirculation Coolers in the Automotive Industry, *Heat Transfer Engineering*, Vol. 32, pp. 248-257.

T.L. Barone, A.A. Lall, Y.F. Zhu, R.C. Yu, and S.K. Friedlander, 2006, Inertial deposition of nanoparticle chain aggregates: Theory and comparison with impactor data for ultrafine atmospheric aerosols, *Journal of Nanoparticle Research*, Vol. 8, 669-680.

Y. Bravo, J. L. Lazaro, and J. Garcia-Bernad, 2005, Study of Fouling Phenomena on EGR Coolers due to Soot Deposits: Development of a Representative Test Method, *Society of Automotive Engineers Technical Paper Series, no.* 2005-01-1143.

J. Hoard, M. Abarham, D. Styles, J. M. Giuliano, C. S. Sluder, and J. M. E. Storey, 2008, Diesel EGR Cooler Fouling, *Society of Automotive Engineers Technical Paper Series, no.* 2008-01-2475.

J. Hoard, J. M. Giuliano, D. Styles, C. S. Sluder, J. M. E. Storey, S. A. Lewis, A. Strzelec, and M. J. Lance, 2007, EGR Catalyst for Cooler Fouling Reduction, *13th Directions in Engine-Efficiency and Emissions Research Conference*, Detroit, MI.

B. Ismail, F. Charles, D. Ewing, J. S. Cotton, and J-S Chang, 2005, Mitigation of the Diesel Soot Deposition Effect on the Exhaust Gas Recirculation (EGR) Cooling Devices for Diesel Engines, *Society of Automotive Engineers Technical Paper Series, no.* 2005-01-0656

A.A. Lall, M. Seipenbusch, W.Z. Rong, and S.K. Friedlander, 2006, On-line measurement of ultrafine aggregate surface area and volume distributions by electrical mobility analysis: II. Comparison of measurements and theory, *Journal of Aerosol Science*, Vol. 37, pp. 272-282.

M.J. Lance, C.S. Sluder, H. Wang, and J.M.E. Storey, 2009, Direct Measurement of EGR Cooler Deposit Thermal Properties for Improved Understanding of Cooler Fouling, *Society of Automotive Engineers Technical Paper Series, no.* 2009-01-1461.

M.J. Lance, C.S. Sluder, J.M.E. Storey, and S.A. Lewis 2010, Characterization of Field-Aged EGR Cooler Deposits, *Society of Automotive Engineers Technical Paper Series, no.* 2010-01-2091.

G. Lepperhoff, and M. Houben, , 1993, Mechanisms of Deposit Formation in Internal Combustion Engines and Heat Exchangers, *Society of Automotive Engineers Technical Paper Series, no.* 931032.

L. Madler, A.A. Lall, and S.K. Friedlander, 2006, One-step aerosol synthesis of nanoparticle agglomerate films: simulation of film porosity and thickness, *Nanotechnology*, Vol. 17, pp.4783-4795.

K. Park, D.B. Kittelson, M.R. Zachariah, and P.H. McMurry, 2004, Measurement of inherent material density of nanoparticle agglomerates, *Journal of Nanoparticle Research,* Vol. 6, pp.267–272.

V. A. Parsegian, 2006, *van der Waals Forces: A Handbook for Biologists, Chemists, Engineers, and Physicists*, Cambridge University press, New York, USA.

C. S. Sluder and J. M. E. Storey, 2008, EGR Cooler Performance and Degradation: Effects of Biodiesel Blends, *Society of Automotive Engineers Technical Paper Series, no.*2008-01-2473.

C. S. Sluder, J. M. E. Storey, and A.. Youngquist, 2009, ULSD and B20 Hydrocarbon Impacts on EGR Cooler Performance and Degradation, *Society of Automotive Engineers Technical Paper Series, no.* 2009-01-2802.

D. Styles, E. Curtis, N. Ramesh, J. Hoard, D. Assanis, M. Abarham, S. Sluder, J. Storey, and M. Lance, 2010, Factors Impacting EGR Cooler Fouling –Main Effects and Interaction, *16th Directions in Engine-Efficiency and Emissions Research Conference*, Detroit, MI.

M. Wiener, G. Reichenauer, S. Braxmeier, F. Hemberger, and H.-P. Ebert, 2009, Carbon Aerogel-Based High-Temperature Thermal Insulation, *International journal of Thermophysics*, Vol. 30, pp. 1372-1385.